CIVIL AND ENVIRONMENTAL ENGINEERING DEPARTMENT

REINFORCED CONCRETE RESPONSE TO

NEAR FIELD EXPLOSIONS

by

T. Michael Baseheart
Civil & Environmental Engineering Department
University of Cincinnati
Cincinnati, Ohio   45221

June 20, 1983

DTIC
ELECTE
DEC 15 1983
S
D

UNIVERSITY OF CINCINNATI
CINCINNATI, OHIO

83 · 12 13 278

Qualified requestors may obtain additional copies from
the Defense Technical Information Service.

Conditions of Reproduction

Reproduction, translation, publication, use and disposal
in whole or in part by or for the United States
Government is permitted.

REPORT DOCUMENTATION PAGE		READ INSTRUCTIONS BEFORE COMPLETING FORM
1. REPORT NUMBER AFOSR-TR- 83-1064	2. GOVT ACCESSION NO. AD-A135876	3. RECIPIENT'S CATALOG NUMBER
4. TITLE (and Subtitle) REINFORCED CONCRETE RESPONSE TO NEAR FIELD EXPLOSIONS		5. TYPE OF REPORT & PERIOD COVERED FINAL 1 Jul 81 - 30 Jun 82
		6. PERFORMING ORG. REPORT NUMBER
7. AUTHOR(s) T MICHAEL BASEHEART		8. CONTRACT OR GRANT NUMBER(s) AFOSR-81-0167
9. PERFORMING ORGANIZATION NAME AND ADDRESS UNIVERSITY OF CINCINNATI DEPT OF CIVIL & ENVIRONMENTAL ENGINEERING CINCINNATI, OH 45221		10. PROGRAM ELEMENT, PROJECT, TASK AREA & WORK UNIT NUMBERS 61102F 2307/D9
11. CONTROLLING OFFICE NAME AND ADDRESS AIR FORCE OFFICE OF SCIENTIFIC RESEARCH/NA BOLLING AFB, DC 20332		12. REPORT DATE June 1983
		13. NUMBER OF PAGES 47
14. MONITORING AGENCY NAME & ADDRESS(If different from Controlling Office)		15. SECURITY CLASS. (of this report) Unclassified
		15a. DECLASSIFICATION/DOWNGRADING SCHEDULE

16. DISTRIBUTION STATEMENT (of this Report)

Approved for Public Release; Distribution Unlimited.

17. DISTRIBUTION STATEMENT (of the abstract entered in Block 20, if different from Report)

18. SUPPLEMENTARY NOTES

19. KEY WORDS (Continue on reverse side if necessary and identify by block number)

BLAST LOADING
REINFORCED CONCRETE
MEMBRANE

20. ABSTRACT (Continue on reverse side if necessary and identify by block number)

From a review of experimental test results for concrete slabs subjected to conventional blast loading, various failure mechanisms and their relationship to scaled breach distance are documented. Analytical studies demonstrate the failure of membrane action when included with the rigid flexural analysis of structural response. For more intense blast pressure intensities, procedures available in the literature are described.

DTIC COPY INSPECTED 3

FINAL REPORT

AFOSR-81-0167

REINFORCED CONCRETE RESPONSE TO

NEAR FIELD EXPLOSIONS

by

T. Michael Baseheart
Civil & Environmental Engineering Department
University of Cincinnati
Cincinnati, Ohio   45221

June 20, 1983

TABLE OF CONTENTS

I. INTRODUCTION

The ever increasing ability of weapons delivery systems to pinpoint their target has prompted survivability analysts and designers to upgrade the resistance capacity of protective structures. A hardened reinforced concrete structure covered by protective layer(s) of soil, concrete burster slab, rock rubble, etc., is required to provide protection against the very high overpressure from the near field, high energy explosion of conventional (non-nuclear) weapons. Conventional weapons detonated near a shallow-buried structure result in a rapidly attenuating, short duration pressure pulse, which is in sharp contrast to the well documented long duration shock front associated with nuclear explosions. The inherent strength, stiffness and stability of boxlike structures makes them suitable for use in such a system. This project is concerned with the dynamic response of reinforced concrete one-way elements, the major structural element of boxlike structures.

Recent experimental testing [1-7] has been performed in an effort to better define the characteristics of underground, non-nuclear explosions, and their effects on underground structures. These model tests provide much needed information about structural failure of reinforced concrete slabs and the in-structure environment to which the personnel, equipment, weapons, etc. would be subjected.

The results of these model tests of reinforced concrete load resisting elements, summarized in Appendix A, indicate that the range of the failure modes vary from the conventional plastic hinge mechanism (standard static response engineering procedure) to material degradation

due to direct intensity of the blast pressure (no structural member response involved). The present work is primarily directed toward the investigation of an approximate analytical model of the failure modes associated with structural member response. Available techniques for theoretically determining direct material degradation characteristics (i.e., spalling) will also be discussed.

Analytical and experimental work in the aeronautical field for years has been devoted to the response of metal beams and plates with solid rectangular cross-sections. Dynamic rigid-plastic theory has been developed for the high intensity loading associated with the blast phenomena. This approach is reasonable when the energy input to the system is significantly larger than the maximum "elastic" strain energy; in other words, the elastic deformations are negligible compared to the plastic deformations.

Simply supported and fixed ended beams without axial restraint, subjected to uniformly distributed impulsive loading, have provided the basis for many investigations. Recently, the temporal and spatial limitations for the loading required by these closed form solutions was overcome by the development of a computer program, CONCRE[8,9], which computes the deflection of the center of a reinforced concrete beam or plate caused by a linear or blast load. Reference 5 provides experimental evidence that buried fixed ended reinforced beams with no axial restraint do exhibit a conventional plastic hinge failure mode, demonstrating that under-reinforced concrete elements possess the necessary ductility for its response to be idealized by a rigid, perfectly

2

plastic constitutive relationship. If the blast pressure is sufficient, the compressive reinforcement, in addition to the tensile reinforcement, may fracture along well defined yield lines, resulting in total disengagement. The sections between hinges essentially remained intact. Because of the lack of in-plane translation restraint on these one-way slabs, the potential membrane capacity of the member is not utilized as it might be in a real boxlike structure.

When the edges, or at least the corners, of a transversely loaded member are restrained against in-plane motion, lateral deflections beyond a certain level ($\Delta \geq 0.3t$) are accompanied by stretching of the middle surface.[10] As the magnitude of the maximum deflection increases, the resulting membrane force can even predominate in providing the lateral load resistance of an axially restrained member. Test results[11] indicate that rectangular cross-section steel beams with full end fixity (flexural plus axial) may develop a static load capacity six or seven times the load carrying capacity of a freely supported beam. Visual examination of the photographic records of laboratory scale blast loading tests by Abrahamson[12] on rectangular cross-section metal beams and plates show maximum deflections that are multiples of the member thickness. For the experimental results of blast loads on reinforced concrete models previously referenced, distinctive yield lines (plastic hinges) are not generally observed to form in the test specimens which are provided in-plane end restraint against translation by their supports.

Much of the more recent analytical efforts have been devoted to

3

describing the response of reinforced concrete elements considering only the flexural, exclusive of the extension, strain energy in their formulation. The inclusion of the effects of an axial restraint in the analysis not only requires additional terms in the differential equation describing the structural response, but also M, the plastic moment capacity of the cross-section, is reduced below M_o, the "full" plastic moment capacity of the cross-section. This capacity reduction depends on the magnitude of N, the tensile force acting on the cross-section. If the intensity of the loading is sufficient to cause N to equal N_o, the "full" plastic tensile capacity of the cross-section, then the flexural capacity M of the cross-section equals zero for the combined loading. With the assumption that the normal tensile force at the location of plastic flow is constant along the member, the succeeding response would resemble that of a plastic string or cable.

This report summarizes a rigid-plastic dynamic analysis procedure for an axially unrestrained beam, then transitions to an investigation of an axially restrained member, which develop internal bending moment and axial force. These procedures, previously developed for ductile metal beams, will be applied to reinforced concrete members.

Loading Cases

Blast loading is characterized by a pulse with an instantaneous rise to a peak positive pressure followed by a decay to zero. This positive pressure duration is followed by a period of negative pressure (suction), as illustrated by the insert in Figure 1. The culmination

4

of considerable effort to document blast load parameters is summarized graphically in the well accepted reference AFM88-22[13]. An abbreviated copy of this graph is provided in Figure 1, where the various blast loading parameters are plotted against the scaled distance $R/W^{1/3}$. These values are for free field air blast, with modifications required to account for the reflection effects when encountered by a structure. A similar widely accepted procedure for underground blast parameters for near field conventional explosions is not available. At this point in the report a brief description of a recently publicized procedure for determining underground blast parameter values is provided.

In recent publications by Southwest Research Institute [7,14], an empirical approach was used to determine underground blast load parameters. A more sophisticated analytical approach was not used because, among other reasons, no recognized equation-of-state are available for different soils exposed to ground shock from nearby detonations. SRI used the pi theorem to determine dimensionless ratios (pi terms) containing the appropriate parameters. Since only dimensionless ratios have to be the same in order for two systems to be equivalent, properly scaled model tests were then used to provide the necessary information to determine the functional format for soil particle velocity, U, and soil displacement, X, in the free field. For example, extensive experimental data illustrated in Figure 2, was used to determine the following function for the soil particle velocity:

$$\frac{U}{c}\left(\frac{P_o}{pc^2}\right)^{0.5} = \frac{0.00617 \left(\dfrac{W_e}{pc^2R^3}\right)^{0.852}}{\tanh\left[26.0 \dfrac{W_e}{pc^2R^3}\right]^{0.30}}$$

with

X = peak radial ground displacement (ft)

U = peak radial ground particle velocity (ft/sec)

R = standoff distance (ft)

W_e = explosive energy release (ft-lb)

p = mass density of the soil or rock (lb-sec^2/ft^4)

c = seismic P-wave velocity in the soil or rock (ft/sec)

P_o = atmospheric pressure (lb/ft^2)

The minimum value of scaled distance for this experimental data is
approximately 2.4, which is sufficient to cause structural mode failure
in buried reinforced concrete members. It is apparent that additional
experimental data is needed to extend this function to a lower limit
for scaled distance.

Using the free field soil particle velocity and the soil displace-
ment, the free field pressure can be approximated. As with obstructions
in air, buried structures are subject to the effects of a reflected[15]
pressure (amplified free field pressure). Experimental evidence is
presently being generated in order to evaluate the effects of the load-
deformation properties of a buried structural element on the magnitude

6

of the reflected pressures felt by the structure. The future utilization of this research will require a more realistic model of the deformational response of the structural elements that comprise buried box structures. Presently, widely used procedures simply double the free field pressures in order to determine the design loads on underground structures. This implicitly assumes that the "rigid" walls terminate the soil particle motion normal to the plane of the wall.

Using a reflected pressure coefficient of 2.0, SwRI published the following equation in reference 14 for the determination of the impulse. applied at any point x on a buried wall.

$$\frac{i(x)}{\rho_s c_p R} = \frac{0.08286 \left(\frac{\rho_s c_p^2}{P_o}\right)^{1/2} \left(\frac{W}{\rho_s c_p^2 (R^2 + x^2)^{3/2}}\right)^{1.105}}{\tanh^{1.5}\left[18.24 \left(\frac{W}{\rho_s c_p^2 (R^2 + x^2)^{3/2}}\right)^{0.237}\right]}$$

Similar equations are presented for the peak reflected pressure distribution. Except for explosions close enough to result in direct material degradation, a valid assumption that greatly simplifies structural response investigations considers blast loadings impulsive. Combined with mass distribution information, the velocity imparted to a structural element can be computed. It should be noted that reference 14 suggests that the mass of the soil between the explosive charge and the structural element be included with the mass of the element in order to obtain a more accurate estimate of the overall dynamic response of the structural element.

While no success was had in locating a published functional relationship for underground blast parameters as the charge location approaches that of a contact charge, this range of scaled distances was addressed for air blasts in a recent publication. Kot et al's[16] procedure, which incorporates the previously referenced air blast parameter values from AFM88-22, is applied to scale distances as small as 0.2, which is well within the deflagration zone of a spherical charge. The spall analysis for this level of intensity of loading is described in a latter section of this report. For now, suffice it to point out that the procedure involves using direction cosines for the components normal to the member along their inclined scaled distance. The temporal variability of these loadings has been ignored as the analysis procedure assumes maximum impulsive loadings irrespective of the time of arrival at the various locations along the member. Short of an extensive finite element/finite difference analysis, considerable determination of the structural response of reinforced concrete members can be had using uniformly distributed loadings in our analysis.

In order to obtain closed form solutions to blast response problems, a considerable amount of the literature is limited to uniformly distributed impulsive transverse loads on flexural members. Considering the arrival time required for near field blast wave to reflect at different locations along the length of a structural member, the complicated loading distribution is certainly not conducive to representation by a single decaying time function. Even Ross' computer program, CONCRE[8,9], which is not constrained to impulsive loadings, does not permit variable

8

temporal functions at different locations along a beam. It should be pointed out that spatial variations allowed in the procedure can result in a theoretical response that violate the inherent requirement in rigid-plastic response that internal moments at all locations along the member not exceed the plastic moment capacity at plastic hinge locations.

The spatial distribution of the blast loading for the determination of the structural response of transversely loaded members in this report will be limited to one that is uniformly distributed. The significance of including membrane effects can be demonstrated without a more exact temporal and spatial definition.

Member Strength

The reinforcement of concrete with ductile steel has long been recognized as a means of overcoming the inherent tensile weakness of concrete when used in a composite structural member. Whitney's Method for computing the ultimate flexural capacity of a cross-section ignores the tensile strength of the concrete and replaces the nonlinear compressive stress distribution (see Figure 3) with a mathematically equivalent rectangular stress block. The same assumption is used to generate interaction diagrams for use with beam-column member capacity determination. As the name of the member implies, a beam-column member is subjected to compressive forces in addition to flexure. An illustration of a typical interaction diagram for a member with longitudinal reinforcement in two parallel faces is provided in Figure 3.[17] Note that M_0 is the pure flexural capacity of the member. In design practice, the steel ratio in

pure flexural equations refers only to the quantity of tensile steel, while in beam-column design aids the steel ratio is based on the total amount of longitudinal steel in the cross-section.

As this work is concerned with the relatively uncommon influence of an axial tension on the response of a flexural member, the typical interaction diagram in Figure 3 is modified to include the combined effects of tension and bending on the member capacity by extending the ordinate on the negative (or tensile) side of the axis. N_0, the maximum value for the tensile force when no bending moment is present, is given by $N_0 = A_{st}F_y$, with F_y equal to the yield strength of the reinforcing steel. Because the concrete will crack before the steel yields, only the steel is assumed to resist the axial tensile force applied to the member at ultimate. The neutral axis position for combined bending and tension is even smaller than its value for pure bending, and when the axial tension is sufficiently large in magnitude, the neutral axis falls theoretically beyond the edge of the cross-section (there is no compression stress in the member). The dashed line in Figure 3 connecting the limiting values for axial tension N_0 and bending moment M_0 illustrates an assumed shape of the interaction diagram for this region. This curve will be approximated in this study by the relationship $(M/M_0) + (N/N_0)^2 = 1$, which is used by Symonds and Mentel[18] to define the relationship between axial tension and bending moment for a solid rectangular ductile cross-section.

The modes of failure of beams and one-way slabs exhibited in field tests with conventional blast loads range from simple plastic

hinge mechanisms through direct material degradation due to the intensity of the compressive blast pressure on the exposed surface of the member. The reason for including the membrane behavior in the analysis is an attempt to explain the severe cracking that accompanies the structural response failure modes even when the intensity of the blast pressure is not sufficient to have caused the damage by either spalling associated with the compressive wave traveling through the member thickness being reflected as a tension stress at the rear free surface, or direct compression blast pressure sufficient to fracture the concrete in the transverse direction due to Poisson's effects. Also when considering the structural response of a member following this initial level of direct material damage to the concrete, only the membrane capacity of the reinforcing steel is available to the member. The behavior of concrete as a material is particularly relevant to comprehending the different failure modes exhibited by the experimental tests. Therefore, even though concrete's tensile strength is not explicitly considered for design purposes, an understanding of concrete tensile strength is required to explain various failure modes.

Flexural Response

References 18 and 19 provide concise documentation of the rigid-plastic response of both simply supported beams and fixed ended beams, with no axial constraint, to a uniform dynamic load $q(x,t) = q(t)$. Consistent with these procedures, the effect of the change of normal and shear forces on the ultimate bending moment are not considered. When the effects of axial restraint are ignored, the rigid plastic solution is quite straightforward. The moment-curvature relationship, ignoring elastic response, results in the basic requirement that no rotation occurs if the internal moment is less than M_o, the full plastic moment capacity of the cross-section. However, unlimited plastic flow can occur if the upper limit moment is maintained at a cross-section.

To review briefly, for a uniformly loaded, simply supported beam, the static collapse mechanism develops a plastic hinge at the beam center. Figure 4a illustrates that the sum of moments about the support yields the static collapse load as $q_s = 8M_o/L^2$. Had the load been applied dynamically, the response would depend upon the intensity of the blast pressure. Consistent with the finding of other investigators, if the maximum intensity of the blast loading is $q_s \leq q \leq 3q_s$, then the failure mechanism is identified as having a single stationary hinge at the center of the beam span, $x = L/2$. Refer to mechanism I in Figure 4a. A consideration of the freebody of the motion results in the following equation for the bending moment on the cross-section at $x = L/2$;[19]

$$M(x_1 t) = M_o \left(\frac{3x}{\ell} - \frac{4x^3}{\ell^3} \right) + \frac{q(t)}{8} \left(\frac{4x^3}{\ell} + \ell x - 4x^2 \right)$$

12

and for the equation of motion[8] of mechanism I:

$$\ddot{\theta} = \frac{3(q(t) + W)}{2m\ell} - \frac{3M_0}{m\ell^3} \qquad 0 \leq t \leq \tau$$

$$\ddot{\theta} = \frac{3W}{2m\ell} - \frac{3M_0}{m\ell^3} \qquad t > \tau$$

For the mechanism to be valid, both halves of the beam must behave as rigid plates, $M(x,t) \leq M_0$.

For more intense dynamic loading, $q > 3q_s$, the structural response deformation pattern in the first phase of motion is given in Figure 4b. Note the two symmetrically located non-stationary plastic hinges. The center portion between the plastic hinges translates vertically with a linear velocity, while the two rigid end segments rotate about their supports. Expressing the continuity of velocity at the intersection of the end segment with the horizontal central section results in the following:

$$\omega a(t) = V$$

Mathematically, the boundary between the segments changes its position during intense dynamic loading, resulting in a bending wave propagation horizontally along the beam (or a moving yield line). The following equation from Henrych's[19] work shows that the boundaries are moving in a direction from the supports towards the center of the beam:

$$a(t) = \sqrt{\frac{6M_0 t}{\int_0^t q(t)dt}}$$

At time $t = t_1$, $a(t_1) = L/2$; therefore, the two hinges are united into a single hinge at the center of the member. The second phase motion,

$t > t_1$, is then simply that of a stationary plastic hinge at the center of the beam, as shown previously in Figure 4a. The time of maximum deflection, t_m, is calculated from the boundary condition of zero velocity. Therefore, for a blast intensity sufficient to initiate a mechanism II response, the value for the maximum deflection at midspan of the member follows directly as the addition of the first and second phase response: $v_{max} = v_1(t_1) + v_2(t_m - t_1)$. The computer program, CONCRE, utilizing numerical integration facilitates the process of actually performing the calculations involved with the various pressure decaying functions that are common to blast loading problems. This computer code also permits spatial loading variations; however, moments exceeding the plastic capacity of the cross-section M_0 may occur between hinges. In Appendix B these equations of motion are derived using the Lagrange equation.

For loadings that can be considered impulsive, $\int_0^t q(t)dt = i$, considerable simplification can be achieved. Consult reference 19 for the closed form solutions of impulsively loaded beams, i.e.,

$$\delta_{final} = \frac{1}{3} \frac{m\ell^2 v^2}{M_0}$$

Beams with Axial Constraints

Symonds and Mentel's[18] rigid-plastic solution procedure for the response of a beam with axial constraints assumes that the normal force N on a cross-section is constant along the member (see Figure 5). Plastic deformations are assumed to occur when M and N satisfy the plasticity

14

criteria that $(M/M_0) + (N/N_0)^2 = 1$.

The flow rule is used to relate the plastic deformations that result when this criteria is satisfied recognizes that the strain rate vector is normal to the yield curve, which is expressed mathematically as

$$\frac{N_0 \dot{\epsilon}}{M_0 \dot{\psi}} = 2 \frac{N}{N_0}$$

where ϵ is the extension strain and ψ is the curvature, and the dot indicates time derivatives.

Considering an intensity of loading sufficient to cause an initial plastic hinge location not at the center of the member, four unknowns, M, N, $\hat{a}$, and ω, will need to be determined. The previously described equations for continuity of velocity at hinge locations and the flow rule relating M and N provide two of the four equations needed. The addition of the axial force effect on the previously examined angular acceleration equation yields

$$\frac{1}{3} ma^3 \dot{\omega} = - M - N \delta$$

where δ is the deflection of the center section of the member. An additional condition resulting from the axial constraint is formulated from a consideration of the rotation of segment AB as it moves through an angle $\Delta\theta$ in a small time interval Δt. This response causes the plastic hinge to move to β with the length of the segment increase by Δx. The curvative change ψ in the segment Δx is given by $\Delta\theta/\Delta x$, and the geometrical requirement in Figure 5 is $\epsilon\Delta x = (\Delta\theta)\delta$.

As formulated by Symonds and Mentel, this relation between extensional

15

strain and curvature change, combined with the flow rule provide the following equation:

$$\frac{N}{N} = \frac{N_o \delta}{2M_o}$$

During the time the hinges are moving toward the center of the member, $\delta = Vt$. Therefore, the initial phase response of mechanism II behavior is found from the solution of simultaneous equations. The result of this is:

$$\frac{mV^3}{6M_o} \frac{d\left(\frac{1}{\omega^2}\right)}{dt} = 1 + \frac{N_o^2 V^2 t^2}{4M_o} \quad ,$$

for which the solution of this differential equation is:

$$\frac{6M_o \omega^2}{mV^3} = \frac{1}{t}\left(1 + \frac{N_o^2 V^2 t^2}{12M_o^2}\right)^{-1} \quad .$$

This initial phase motion terminates at time t_1, when $a(t) = \ell$, with $\omega\ell = V$. Therefore

$$t_1 = \frac{mV\ell^2}{6M_o}\left(1 + \frac{N_o^2 V^2 t_1^2}{12M_o}\right)^{-1}$$

The two halves of the beams (rigid bars) then rotate about the supports during the second phase. The permanent curve change and axial extensions are assumed to occur at the plastic hinge at midlength of the beam. The unknown quantities are M, N, $\omega = \dot{\theta}$, and δ. The same four simultaneous equations as for the initial phase response are solved with $a(t) = \ell$ (plastic hinge at midspan). The solution of the resulting differential equation, and simplification of the results in reference 18 furnishes

the following equation for the final deflection δ_f

$$\frac{\delta_f}{\ell} + \beta^2 \left(\frac{\delta_f}{\ell}\right)^3 = 2\alpha$$

where the dimensionless parameter $\quad \beta \equiv \dfrac{N_0 \ell}{12 M_0}$

and $\qquad\qquad\qquad\qquad\qquad \alpha \equiv \dfrac{m \ell V^2}{6 M_0}$

For beams with fixed ends, the final deflections can be determined simply by replacing M_0 with $2M_0$ in the equations for final deflections. This rather simple analysis provides results for the effect of axial restraint on the transverse response of beams assuming rigid plastic behavior. However, the foregoing procedure is valid only so long as $N/N_0 < 1$. At succeeding intervals of time, the axial force probably remains constant and equal to N_0, which establishes the bending moment is zero throughout the beam. The classical partial differential equation describing the future behavior of the member as a plastic string is:

$$\frac{\partial^2 y}{\partial x^2} = \frac{m}{N_0} \frac{\partial^2 y}{\partial t^2}$$

For the details of the derivation of the response of a member in the plastic string phase you are referred to section 4 of reference 18. The approximate conservative solution from this publication is given by the following equation

$$\frac{\delta_f}{\ell} < V\sqrt{\frac{m}{N_0}} - \frac{M_0}{N_0 \ell}$$

The following example problem is used to illustrate the relative magnitude of deflection when axial constraint is considered in the analysis.

Simply Supported Concrete Beam with Symmetrical Tensile and Compressive Steel

Span = L = 80 in. $\qquad f_c^{\prime}$ = 6.0 ksi

Depth = t = 6 in. $\qquad f_y$ = 60.0 ksi

Width = b = 12 in.

Steel Ratio = p_t = 0.01

Cover for
Steel = 0.75 in.

Ratio of distance between centroid of outer rows of

bars and the depth of the cross-section = γ = 0.75

Properties of cross-section:

m = mass per unit length

$$= \frac{(12 \text{ in. x 6 in.})(0.083 \text{ lb/in}^3)}{386 \text{ in/sec}^2} \times \frac{1 \text{ kip}}{1000 \text{ lb.}}$$

m = 15.5 x 10^{-6} $\frac{k - sec^2}{in}$ per inch length of member

N_o = Axial Yield Capacity

$\quad = A_s f_y = p_t A_g f_y = (0.01 \times 72 \text{ in}^2)(60 \text{ K/in}^2)$

N_o = 43.2 kips

M_o = Pure Moment Capacity of Cross-section

Using the ACI interaction diagrams[17], the pure flexural capacity

for this doubly reinforced cross-section is determined from the following

equation and appropriate moment coefficient:

$$\frac{\phi M_o}{A_g t} = 0.2331$$

For a capacity reduction factor $\phi = 1$, the flexural capacity $M_o = 100.7$ in-k.

For an initial velocity V_o equal to 500 in/sec imparted to the beam by an impulsive blast load,

with no axial constraint:

$$\frac{\delta_f}{\ell} = \frac{m\ell V_o^2}{3M_o}$$

$$= \frac{(15.5 \times 10^{-6} \frac{\text{k-sec}^2}{\text{in}^2})(40 \text{ in})(500 \text{ in/sec})^2}{3 (100.7 \text{ in-k})}$$

$$\frac{\delta_f}{\ell} = 0.51$$

with axial constraint:

$$\frac{\delta_f}{\ell} = V_o \sqrt{\frac{m}{N_o}} - \frac{M_o}{\ell N_o}$$

$$= 500 \text{ in/sec} \sqrt{\frac{15.5 \times 10^{-6} \frac{\text{k-sec}^2}{\text{in}^2}}{43.2^k}} - \frac{100.7 \text{ in-k}}{(40 \text{ in})(43.2 \text{ k})}$$

$$\frac{\delta_f}{\ell} = 0.24$$

Figure 6 illustrates the effects of the initial velocity on the relative magnitude of the final midspan deflection when axial restraint is considered. The curve demonstrates that for a typical reinforced concrete member the deflections calculated for a simply supported unrestrained beam will be much larger than the deflections determined for an axially restrained beam. Even though these results are based on an approximate procedure, it is certainly appropriate for design procedures.

In order to utilize the previous information, a failure criteria must be determined to relate the rupture of the reinforcing steel to the midspan deflection δ_f. From standard assumptions relative to membranes, the following equation for the longitudinal strain in the reinforcing steel is:

$$\epsilon_x = \frac{1}{2}\left(\frac{\partial \delta}{\partial x}\right)^2$$

An assumed mode shape during the membrane response is given by:

$$\delta = \delta_f \cos \frac{\pi x}{2\ell} \qquad ,$$

where x is measured from the midspan of the member. The strain can now be expressed in terms of the midspan deflection, δ_f.

$$\epsilon_x = \frac{\pi^2 \delta_f^2}{8\ell^2} \sin^2\left(\frac{\pi x}{2\ell}\right)$$

This equation is maximum at $x = \ell$ which corresponds to the support location.

$$(\epsilon_x)_{max} = \frac{\pi^2 \delta_f^2}{8\ell^2}$$

Rearranging:

$$\frac{\delta_f}{\ell} = \frac{2}{\pi}\sqrt{2\,(\epsilon x)_{max}}$$

From ASTM A615, the tensile specifications for Grade 40 and Grade 60 reinforcing steel require material elongations $(\epsilon_x)_{max}$ from 8% to 11% for the size reinforcing bars normally used in blast resistant structures. For this example problem the steel would theoretically rupture in the axially restrained member at (δ_f/ℓ) values of 0.255 and 0.298, respectively.

Spalling of Concrete Walls

When computing the structural response of reinforced concrete elements to intense blast, authors have invariably ignored the loss of the composite properties of the cross-section due to spallation, etc. While the structural response is generally considered as a reaction to impulsive loads, several internal stress wave reflections associated with spalling have occurred before the structural motion begins. As a consequence, the small sized, high velocity spall debris (normally considered to be comprised of the concrete cover over the reinforcement. on the back side of the wall) has been discharged before the overall structural motion has commenced. As stated in reference 16, the smaller velocity imparted to the larger spall particles causes them to stay with the structural element and to be ejected later by the larger wall velocities associated with structural response.

The immediately occurring extensive internal damage to the concrete associated with the internal tension stresses resulting from the reflected compressive blast waves would most certainly eliminate the flexural capacity of the member. The structural motion resistance would then be limited to the membrane capacity of the reinforcing steel.

Literature documenting an analytical procedure for determining spallation of underground walls was not found; however, comprehensive references on spallation as the result of air blast on a structural wall were discovered. The principles applied to these walls apply equally well to a buried wall, with the exception that the relationship between charge weight, standoff distance, and the resulting load parameters

(i.e., pressure, impulse, etc.) would be different. For both situations, identical loading parameters on a wall would yield equivalent responses.

The analytical work done on this subject that is referenced here required considerable simplification of a very complex problem. The basis for the simplified analysis is well known and is simply restated here from reference 16. "The phenomena of spall in brittle materials occurs when strong tension waves are reflected into the wall from the free surface at the back face and interact with the decaying compression wave in such a way as to produce locally tension stresses which exceed the dynamic tensile rupture strength of the material." An estimate of the threshold was proposed in reference 14 using the following assumptions: (1) uniform loading of wall, (2) triangular pressure-time history, which directly relates the peak reflected pressure P_r, reflected positive specific impulse i_r, and positive pulse duration T, (3) no attenuation of the pressure wave through the wall, and (4) a stress wave velocity through the wall given by $v = \sqrt{E/\rho}$, where E is Young's Modulus and ρ is density. The results of this analysis for predicting the threshold of spallation from reference 14 are reproduced in Figure 7. A more in depth analysis is required to predict spall size and spall velocity.

Kot et al.[16] studied spalling effects for large, thick concrete elements associated with power plant structures. Unlike the previous described reference, the decay of the peak pressure through the wall and the non-uniform nature of the blast loading are considered. The later factor takes into consideration the added complication of the spalling

of concrete due to normal and oblique incidence, with the determination that no spall is anticipated for incidence angles greater than 45°. The set of graphs available in reference 16 is not directly applicable to buried structures as the blast load parameters for scaled distances were obtained from AFM88-22[13]. However, similar response would be observed for buried structures with comparable loading functions. Several scaled graphs are presented which relate spall thickness, spall number, and spall velocity to scaled distance, wall thickness, angle of incidence, etc. Some important conclusions can be documented as a consequence of the analysis of material presented in reference 16.

For walls where no attenuation of the shock wave in the wall is assumed to take place, spall thickness depends on the assumed profile of the compression blast wave. Since the blast wave is steepest at the shock front and becomes less steep as the peak pressure decays, the first spall is the thinnest. However, it also possesses the highest velocity. The authors also note that the total depth of spall is nearly constant, being approximately equal to one half the wave length of the compression wave. Also, the angle of incidence has a pronounced effect on spall thickness and velocity. Kinetic energy per unit area for oblique incidences is substantially larger than for normal incidence. When the wall thickness effects on decay of the blast loading intensity is considered, the spall thickness increases with increasing wall thickness while the spall velocity decreases.

Kot et al.[16] also computed the structural response in the form of wall displacements for impulsive loads. A circular yield line pattern

is assumed to form in a large structural wall. The radius of this yield pattern is determined by evaluating circles with incrementally larger radii until the maximum value of deflection is determined. A graph from reference 16 showing scaled concrete wall velocities due to impulsive air blast loading is given in Figure 8. This graph illustrates the coupling between spalling and wall motion which results in high velocity ejection of most spall debris. It should be pointed out that modeling the structural response by ultimate strength yield line procedures requires that the cross-section possess flexural capacity, which in reality is destroyed by the preceeding spallation. This leaves the member with only the membrane capacity of the reinforcing steel.

Conclusions

The extension of the rigid plastic analysis procedure to include the effects of axial constraint on the member's response furnishes an important previously overlooked link necessary to explain a range of experimentally observed failure modes. The extension strain consistent with axial restraint provides an explanation for the experimental response observed where the overall deflection is not excessive, but the damage to the concrete is extensive. The initial material degradation due to the intensity of the blast pressure oscillations would destroy the flexural capacity of the composite cross-section, leaving only the membrane capacity of the reinforcing steel to determine the structural response. While the approximate closed form analysis procedure presented demonstrates the significance of including membrane response, there is definitely the

24

need to develop a more sophisticated numerical technique in order to examine the effects of extension strain more closely.

REFERENCES

1. Kiger, S.A., and Albritton, G.E., "Response of Buried Hardened Box Structures to the Effects of Localized Explosions," Technical Report SL-80-1, March, 1980, U.S. Army Engineer Waterways Experimental Station Structures Laboratory, Vicksburg, Miss.

2. Fuehrer, H.R., and Keeser, J.W., "Breach of Buried Concrete Structures," AFATL-TR-78-92, USAF Armament Lab., Eglin AFB, Fl., August, 1978.

3. Fuehrer, H.R., and Keeser, J.W., "Response of Buried Concrete Slabs to Underground Explosions," AFATL-TR-77-115, USAF Armament Lab., Eglin AFB, Fl., Sept., 1977.

4. Fuehrer, H.R., and Keeser, J.W. "Investigation of Oblique Shocks and Edge Effects for Underground Targets," AFATL-TR-77-1, Volume 11, USAF Armament Lab., Eglin AFB, Fl., Jan., 1977.

5. Kiger, S.A., and Hossley, J.R. "Field Test of a Buried Hardened Structure Subjected to a Cylindrically Cased Equivalent Charge," Misc. Paper N-77-8, August, 1977, U.S. Army Engineers Waterway Experiment Station Weapons Effects Laboratory, Vicksburg, Miss.

6. Kiger, S.A., "Static Test of a Hardened Shallow-Buried Structure," Technical Report N-78-7, Oct., 1978, U.S. Army Engineer Waterways Experiment Station Weapons Effect Laboratory, Vicksburg, Miss.

7. Esparza, Edward D., Westine, Peter S., and Wenzel, Alex B., "Pipeline Response to Buried Explosive Detonations," Vol. II, American Gas Association Project PR-15-109 (SWRI Project 02-5567), Southwest Research Institute, San Antonio, Texas, August, 1981.

8. Ross, C.A., and Schaubb, C.C., "Failure of Underground Hardened Structures Subjected to Blast Loading," AFSOR783592, USAFOSR, Bolling AFB, D.C., April 1979.

9. Ross, C.A., Nash, P.T., and Griner, G.R., "Failure of Underground Concrete Structures Subjected to Blast Loadings," The Shock and Vibration Bulletin, Bulletin 49, Part 3, Sept., 1979, p. 1-9.

10. Szilard, R., Theory and Analysis of Plates, Prentice-Hall, Inc., 1974, p. 340.

11. Haythornthwaite, R.M., "Beams With Full End Fixity," Engineering, January 25, 1957, p. 110-112.

12. Abrahamson, G.R., Florence, A.L., and Lindberg, H.E., "Radiation Damage Study (RADS) - Vol XIII, Dynamic Response of Beams, Plates and Shells," BSDTR66-372, Vol XIII, Ballistics Systems Div., Norton AFB, CA., Sept., 1966.

13. _Structures to Resist the Effects of Accidental Explosions_, Department of the Army Technical Manual TM5-1300, Department of the Navy Publication NAVFAC P-397, Departmentof the Air Force Manual AFM88-22, Department of the Army, the Navy and the Air Force, June 1969.

14. Baker, W.E., Westine, P.S., Kulesz, J.J., Wilbeck, J.S. and Cox, P.A., "A Manual for the Prediction of Blast and Fragment Loading on Structures," (1980), DOE/TIC-11268, U.S. Dept. of Energy, Amarillo, TX, Nov. 1980.

15. Vretblad, Bengt E., "Response of Structures to Detonations in Sand," Proceedings of the Symposium on the Interaction of Non-Nuclear Munitions with Structures, U.S. Air Force Academy, Colorado, May 1983.

16. Kot, C.A., Valentin, R.A., McLennan, D.A., and Turula, P., "Effects of Air Blast on Power Plant Structures and Components," NUREG/CR-0442, U.S. Nuclear Regulatory Commission, Oct. 1978.

17. _Design Handbook - Vol. 2 - Columns_, Publication SP-17A(78), American Concrete Institute, Detroit, Michigan, 1978.

18. Symonds, P.S., and Mentel, T.J., "Impulsive Loading of Plastic Beams with Axial Constraints," _Journal of the Mechanics and Physics of Solids_, Vol. 6, 1958, p. 186-202.

19. Henrych, Josef, _The Dynamics of Explosion and Its Use_, Elsevier, New York, 1979.

20. Symonds, P.S., "Elastic, Finite Deflection and Strain Rate Effects in a Mode Approximation Technique for Plastic Deformation of Pulse Loaded Structures," _Journal Mechanical Engineering Science_, Vol. 22, No. 4, 1980, p. 189-197.

21. Karthaus, W., and Levssink, J.W., "Dynamic Loading: More Than Just A Dynamic Load Factor," Proceedings of the Symposium on the Interaction of Non-Nuclear Munitions with Structures, U.S. Air Force Academy, Colorado, May 1983.

22. Crawford, R.E., "Protection From Non-Nuclear Weapons," Technical Report AFWL-TR-70-127, AFWL, Kirkland AFB, N.M., Feb., 1971.

APPENDIX A

A review of numerous experimental test reports revealed significant differences among test specimens, their restraint and loading conditions, and the interpretation of breach loading conditions. The later is to be expected considering the different failure modes possible for reinforced concrete slabs that are subjected to blast pressures that range in magnitude from slightly above the static collapse load to several times larger than f'_c, the statically determined cylinder strength of concrete. Therefore, no attempt is made to arbitrarily define breach conditions. Rather, test specimens that sustained severe damage are classified according to their apparent mode of failure.

The failure test data used in this report is given in Tables 1 and 2. The information in Table 1 was used in reference 3 to obtain the previously stated empirical breach equation, while Table 2 contains additional test data presently available. From an examination of the test data and photographs of these specimens, the following failure mechanisms are delineated based on the type and degree of damage:

(1) Yield Line, without concrete degradation,

(2) Yield line, with concrete degradation,

(3) Membrane, with severe spalling or scabbing,

(4) Direct concrete crushing and spalling, with membrane net,

(5) Shear, and

(6) Overbreach.

These assumed failure response mechanisms have the following characteristics.

Yield Line, without concrete degradation. This mechanism is characterized by plastic hinge formation at points of maximum flexural stress with the sections of the member between hinge lines remaining essentially intact. Under-reinforced concrete elements possess the necessary ductility for its response to be idealized by a rigid, perfectly plastic, constitutive relationship. This flexural failure is characterized by crushing of the concrete along the yield line in the flexural compression zone of the crossection. The depth of this concrete loss is not excessive because concrete slabs are usually con-siderably under-reinforced. With tied compressive reinforcement present, the member continues to respond in this flexural mode until fracture occurs due to excessive straining of the tension reinforcement. For severe overloads, the compressive reinforcement may also fracture, resulting in total disengagement

tween hinges.

.ield Line, with concrete degradation. In addition to the previously described
flexural failure associated with the formation of the plastic hinge(s),
concrete failure occurs directly due to the intensity of the blast pressure.

Membrane, with severe spalling or scabbing. When the edges, or at least the
corners, of a slab are restrained against in-plane motion, lateral deflections
beyond a certain level ($\Delta \geq 0.3$ t) are accompanied by stretching of the middle
surface[10]. As the magnitude of the maximum deflection increases, the resulting
membrane force can significantly aid or even predominate in carrying the lateral
loads. The final deflected shape of reinforcing steel in test specimens failed
with this mechanism is consistent with the shape observed for pure membranes
subjected to distributed loads. The analytical and experimental results of ref-
erence 11 support the concept of this membiane type failure response for thin,
fixed-edge flat plates subjected to explosive pressure loadings. Spalling,
which is caused by the shock pressure of a blast being transmitted through an
element, results in a tension failure in the concrete normal to its free
surface. Scabbing is also a tensile failure of the concrete, but is associated
with the large strains in the reinforcement at the later stages of ductile
response of a reinforced concrete element. The velocities of scabbed fragments
of concrete are lower than the velocities of spalling fragments.

Direct concrete crushing and spalling, with membrane. The following description
from reference 22 of the response of a member to a contact explosion also
describes the mode of failure under consideration. Near the point of detonation,
the magnitude of the compressive pulse is sufficient to crush the concrete
material. The pulse decays rapidly as it propagates through the member until
no additional crushing is possible or the structure is breached. If the later
does not occur, a compression wave is reflected by the inner surface as a
tension pulse wave. If the tensile strength of the concrete is exceeded,
rupture will occur and the spall will fly off in response to the trapped mo-
mentum. Additional ejection of crushed and spalled material occurs as the tension
wave propagates back to its point of detonation. The flexural capacity of the
member is lost, leaving only the membrane capacity of the reinforcing net.

<u>Shear</u>. This is a catastrophic failure mode in which there is very little evidence of flexural behavior. The affected area of wall is typically blown into the structure nearly intact, with boundaries showing direct shear failure, rather than diagonal tension failure.

<u>Overbreach</u>. Catastrophic damage is obvious, with concrete disentegrated and blown away. The reinforcing steel does not span the opening and is in disarray.

Figure A1 shows the different slab support configurations used in the various testing programs. The experimental breach data is plotted in Figure A2 with each data point symbol indicating the failure mechanism for that test specimen.

Except for one test, the data for $\lambda \geq 1.4$ consists entirely of the results from slabs supported on two legs. The slabs in these tests fail in flexural through the formation of yield lines. The author observed that because of the lack of in-plane translation restraint on the slab, the membrane capacity of the slab is not utilized as it might be in a real box structure. The distinctive yield line (plastic hinge) is not observed to form in any of the test specimens which are provided in-plane restraint against translation by their supports.

Tables 1 and 2 indicate that the majority of the test specimens contain considerably less steel reinforcement than one would expect to find in actual hardened structures. No reference that attributes this reduced reinforcement value to model scaling was found. While conservative, the use of steel ratios significantly less than that of actual structures should have a pronounced effect on the specimens with the larger breach loading distances where structural member response, rather than direct crushing of the concrete material, is the primary cause of failure.
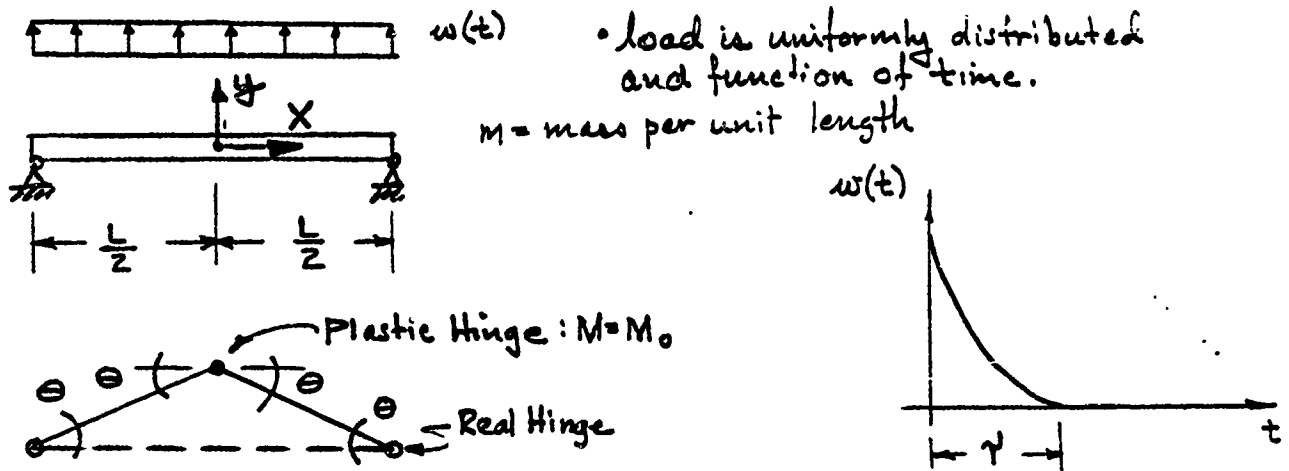
For scaled breach distances less than 1.4 there appears to be direct material degradation present due to the initial intensity of the blast pressure on the restrained test specimens. The two test specimens in this range that did fail without direct material crushing are unrestrained two-legged test specimens. These two specimens also contain a steel ratio $\rho = 0.0025$ for the tensile reinforcing steel in one direction. This definition for steel ratio, consistent with conventional reinforced concrete practice, is equal to one-fourth of the amount reported in reference 2 as the volume of steel in the

specimen. This minimal amount of reinforcement, equivalent to what is normally considered an amount of steel simply for temperature and shrinkage control, probably accounts for the unexpected yield line failure mechanism in the high intensity range of scaled breach distances. It should be pointed out that the yield line failure mechanism would appear essentially the same as a modulus of rupture type failure typical of a concrete flexural member that is effectively unreinforced.

Equations of Motion Derived Using the Lagrange Equation

FOR A PINNED-PINNED BEAM WITH STATIONARY HINGE:

$w(t)$

- load is uniformly distributed and function of time.

$m =$ mass per unit length

Plastic Hinge : $M = M_0$

Real Hinge

Assume Rigid-Plastic Plastic Behaviour.

- displacement of any point is a funtion of time and X.

- let y_0 indicate the time-varying displacement at $X = 0$.

Then $y(t) = f(y_0) = \begin{cases} y_0 - 2y_0 X/L & \text{for } X \geq 0 \\ y_0 + 2y_0 X/L & \text{for } X \leq 0 \end{cases}$

$\underline{K}$

Kinetic Energy of beam, $K = \int_{-L/2}^{L/2} \frac{1}{2} m \dot{y}^2 dX = 2 \int_{0}^{L/2} \frac{1}{2} m \dot{y}^2 dX$

$K = m \int_{0}^{L/2} \dot{y}^2 dX = m \int_{0}^{L/2} \left(\dot{y}_0 - \frac{2\dot{y}_0}{L} X \right)^2 dX$

$\boxed{K = \frac{1}{6} m \dot{y}_0^2 L}$

$\underline{S}$

Plastic Strain Energy, $S = M (2\theta)$

$\theta = 2y_0/L$

$\boxed{S = 4 \dfrac{M_0 y_0}{L}}$

32

$\underline{\underline{W}}$. External Work due to external forces

$$dW = \omega(t)\,dX\,dy \qquad dy = \left(1 - \frac{2X}{L}\right)dy_0 \quad \text{for } X \geq 0$$

$$W = 2\int_0^{y_0}\int_0^{L/2} \omega(t)\left(1 - \frac{2X}{L}\right)dX\,dy_0$$

$$\boxed{W = \tfrac{1}{2}\,y_0\,L\,\omega(t)}$$

LAGRANGE EQUATION IS: $\dfrac{d}{dt}\left(\dfrac{\partial G}{\partial \dot{q}}\right) - \dfrac{\partial G}{\partial q} = Q$

- in which $G = K - S$
- let q be the generalized coordinate y_0
- $Q = \dfrac{\partial W}{\partial q} = \tfrac{1}{2}L\,\omega(t)$

The indicated substitutions give

$$\tfrac{1}{3}m\ddot{y}L + \frac{4M_0}{L} = \tfrac{1}{2}L\,\omega(t)$$

or

$$\boxed{\ddot{y}_0 = \frac{3}{2m}\,\omega(t) - \frac{12M_0}{mL^2}}$$

FOR A FIXED-FIXED BEAM WITH STATIONARY HINGE:
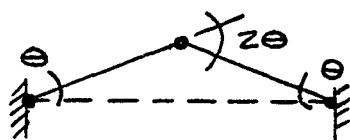
$$\boxed{K = \tfrac{1}{6}\,m\,\dot{y}_0^2\,L}$$

Kinetic Energy same as for pinned-pinned beam.

$\underline{\underline{S}}$ Plastic Strain Energy, $S = M_0(4\theta)$ and $\theta = 2y_0/L$

$$\boxed{S = 8\,\frac{M_0 y_0}{L}}$$

$\underline{\underline{W}}$ External Work $\boxed{W = \tfrac{1}{2}y_0 L\,\omega(t)}$ as for pinned-pinned b''

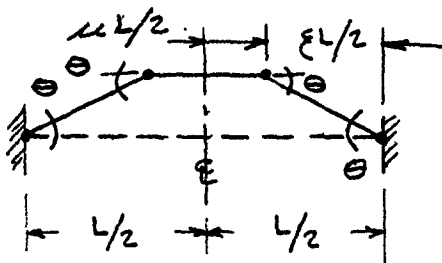$$Q = \frac{\partial W}{\partial y_0} = \frac{1}{2} L \omega(t)$$

LAGRANGE EQUATION, $\frac{d}{dt}\left(\frac{\partial G}{\partial \dot{q}}\right) - \frac{\partial G}{\partial q} = Q$, GIVES

$$\frac{1}{3} m \ddot{y}_0 L + 8 \frac{M_0}{L} = \frac{1}{2} L \omega(t)$$

or

$$\boxed{\ddot{y}_0 = \frac{3}{2} \frac{\omega(t)}{m} - \frac{24 M_0}{m L^2}}$$

FOR A FIXED-FIXED BEAM WITH A TRAVELING HINGE MECHANISM:

NOTE: $\mu = 1 - \xi$
$\quad\quad \ell = L/2$

$$\theta = \frac{2 y_0}{(1-\mu) L}$$

$$y = \begin{cases} y_0 & \text{for } 0 \leq X \leq \frac{\mu L}{2} \\[2mm] y_0 \left[\dfrac{L - 2X}{(1-\mu) L}\right] & \text{for } \frac{\mu L}{2} \leq X \leq \frac{L}{2} \end{cases}$$

$\underline{\underline{K}}$ Kinetic Energy of Beam, $K = \int_{-L/2}^{L/2} \frac{1}{2} m \dot{y}^2 \, dX = 2 \int_0^{L/2} \frac{1}{2} m \dot{y}^2 \, dX$

$$\therefore K = \int_0^{\mu L/2} m \dot{y}_0^2 \, dX + \int_{\mu L/2}^{L/2} m \dot{y}_0^2 \left[\frac{L - 2X}{(1-\mu) L}\right] dX$$

$$\boxed{K = \frac{m \dot{y}_0^2 L}{6} \left[1 + 2\mu\right]}$$

$\underline{\underline{S}}$ Plastic Strain Energy, $S = M_0 (4\theta)$ and $\theta = \frac{2 y_0}{(1-\mu) L}$

$$\boxed{S = \frac{8 M_0 y_0}{(1-\mu) L}}$$

$\underline{\underline{W}}$ External Work

$$dW = w(t)dX\,dy \qquad\qquad dy = \begin{cases} dy_0 & \text{for} \quad 0 \le X \le \frac{\mu L}{2} \\[2mm] \left[\dfrac{L-2X}{(1-\mu)L}\right]dy_0 & \text{for} \quad \frac{\mu L}{2} \le X \le \frac{L}{2} \end{cases}$$

$$W = \int_0^{y_0}\int_{-L/2}^{L/2} w(t)dX\,dy = 2\int_0^{y_0}\int_0^{L/2} w(t)\,dX\,dy$$

$$W = 2\int_0^{y_0}\int_0^{\mu L/2} w(t)\,dX\,dy_0 + 2\int_0^{y_0}\int_{\mu L/2}^{L/2} w(t)\left[\frac{L-2X}{(1-\mu)L}\right]dX\,dy_0$$

$$\boxed{W = \tfrac{1}{2}(1+\mu)\,w(t)\,y_0 L}$$

$$Q = \frac{\partial W}{\partial y_0} = \tfrac{1}{2}(1+\mu)\,w(t)L$$

LAGRANGE. EQUATION, $\frac{d}{dt}\left(\frac{\partial G}{\partial \dot{q}}\right) - \frac{\partial G}{\partial q} = Q,$ GIVES

$$\tfrac{1}{3}m\ddot{y}_0 L(1+2\mu) + \frac{8M_0}{(1-\mu)L} = \tfrac{1}{2}(1+\mu)\,w(t)L$$

or

$$\boxed{\ddot{y}_0 = \frac{3}{2}\frac{w(t)}{m}\left(\frac{1+\mu}{1+2\mu}\right) - \frac{24 M_0}{mL^2(1+2\mu)(1-\mu)}}$$

For the center portion alone, because the shear force is zero at the internal hinges, it can be shown that

$$\ddot{y}_0 = \frac{w(t)}{m}$$

Equating the last two equations gives

$$\frac{w(t)}{m} = \frac{3}{2}\frac{w(t)}{m}\left(\frac{1+\mu}{1+2\mu}\right) - \frac{24 M_0}{mL^2(1+2\mu)(1-\mu)}$$

which can be solved for μ as

$$\mu = 1 - \left[3w^*/w(t)\right]^{1/2}$$

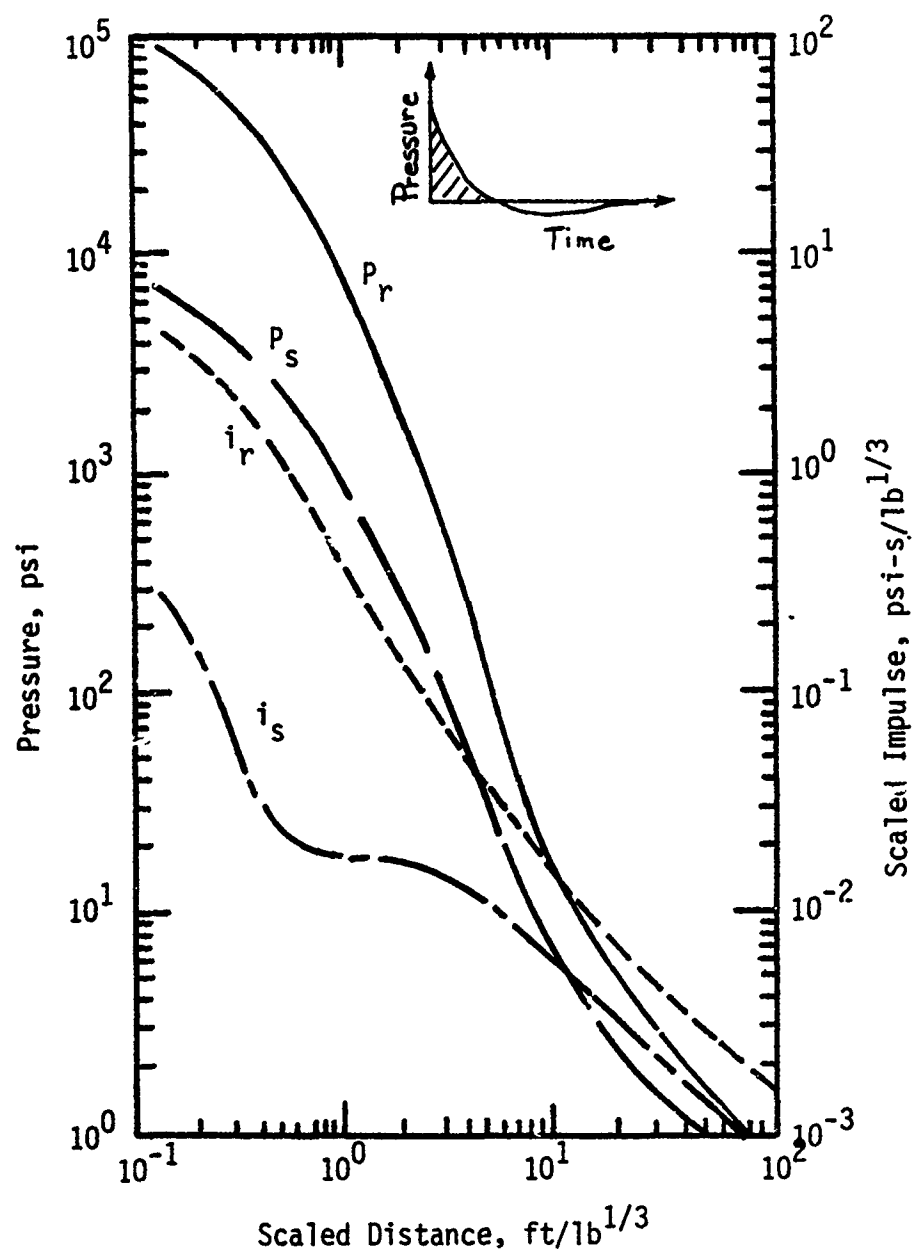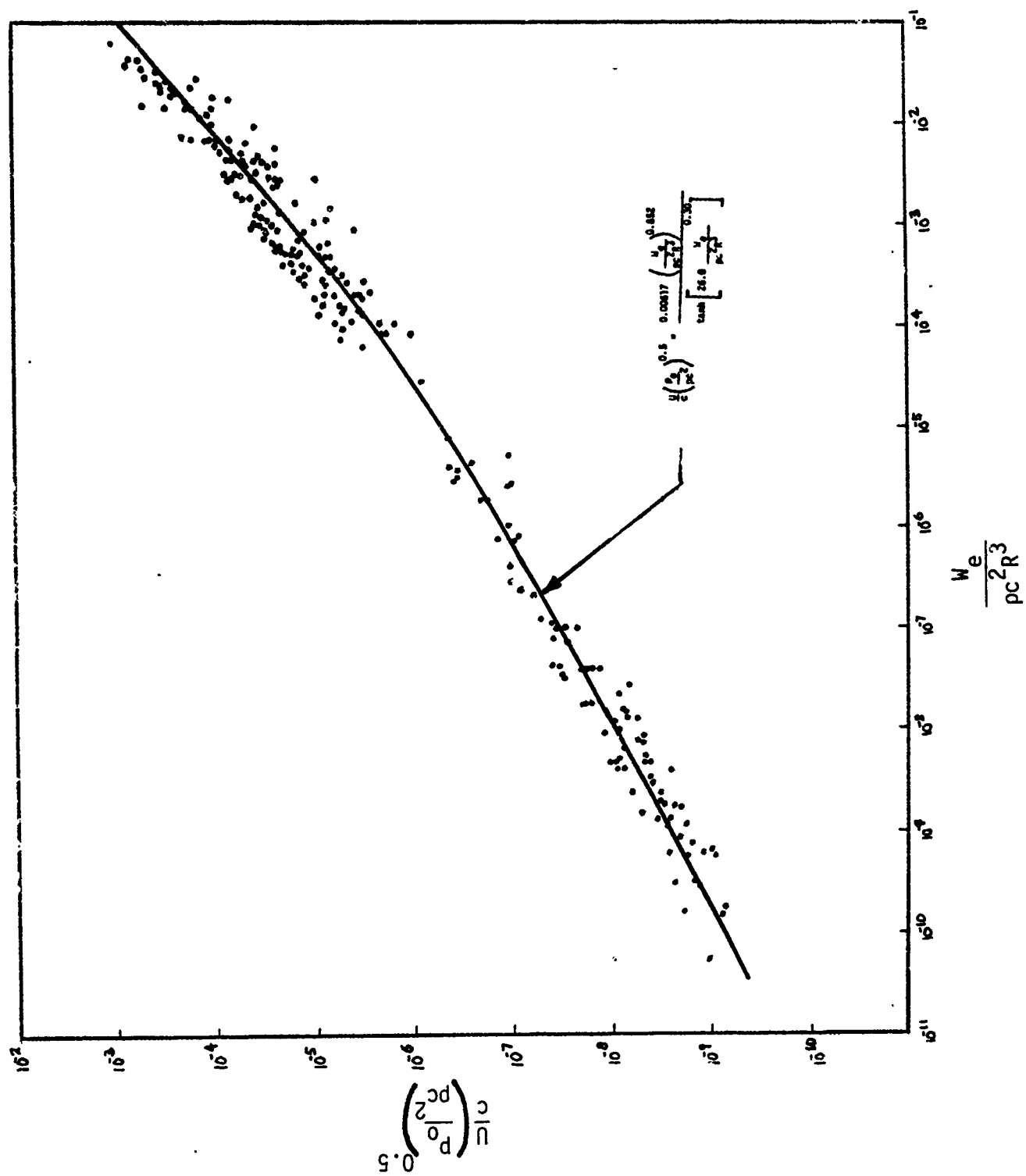where $w^* = \dfrac{16 M_0}{L^2}$, the static collapse load.

35

Figure 1. Air Blast variables (From Reference 13,16)

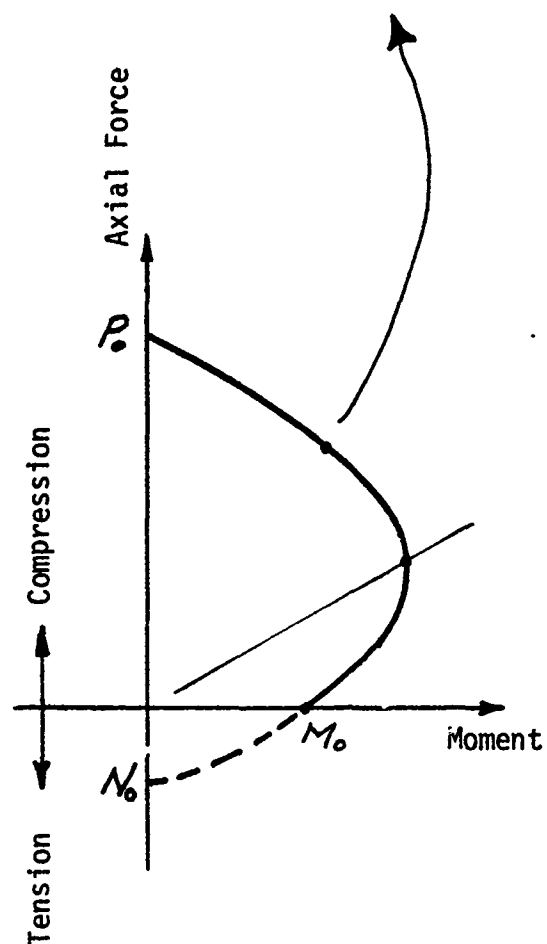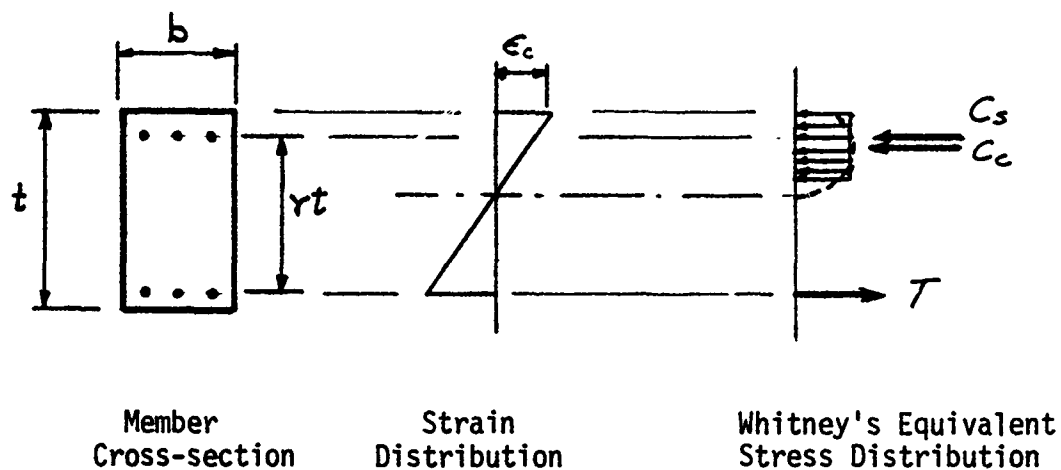$$\frac{U}{c}\left(\frac{\rho_o}{\rho c^2}\right)^{0.5} = \frac{0.00017 \left(\frac{W_e}{\rho c^2 R^3}\right)^{0.642}}{\tanh\left[26.0 \frac{W_e}{\rho c^2 R^3}\right]^{0.35}}$$

$$\frac{W_e}{\rho c^2 R^3}$$

$$\frac{U}{c}\left(\frac{\rho_o}{\rho c^2}\right)^{0.5}$$

37

Member
Cross-section

Strain
Distribution

Whitney's Equivalent
Stress Distribution

Figure 3. Strength Interaction Diagram Showing Both
Axial Compression and Axial Tension
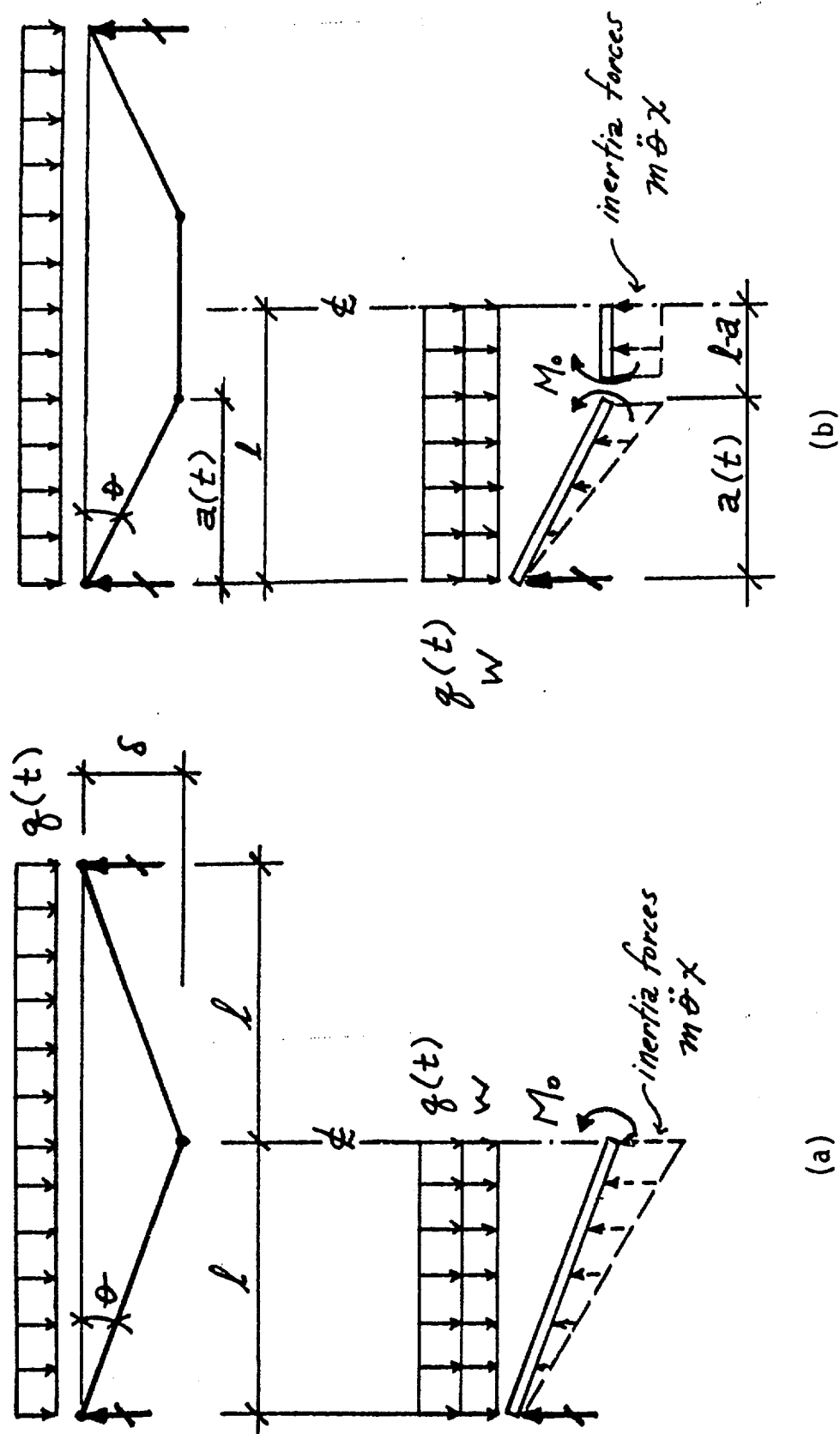
Figure 4. Simple beam: (a) Stationary deformations and forces (b) Non-stationary deformations and forces.

39

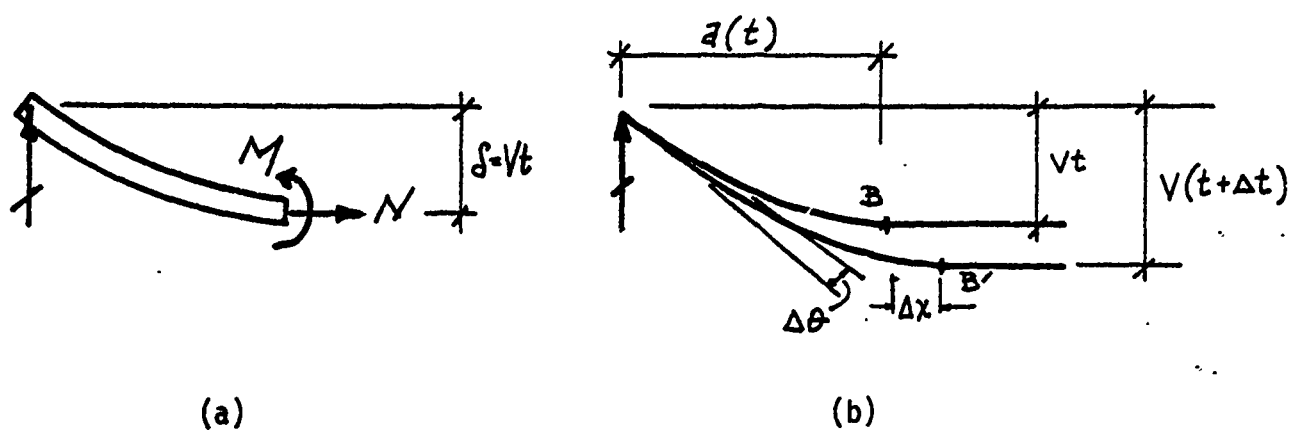(a)   (b)

Figure 5. Simple Beam with Axial Constraint   (a) Forces
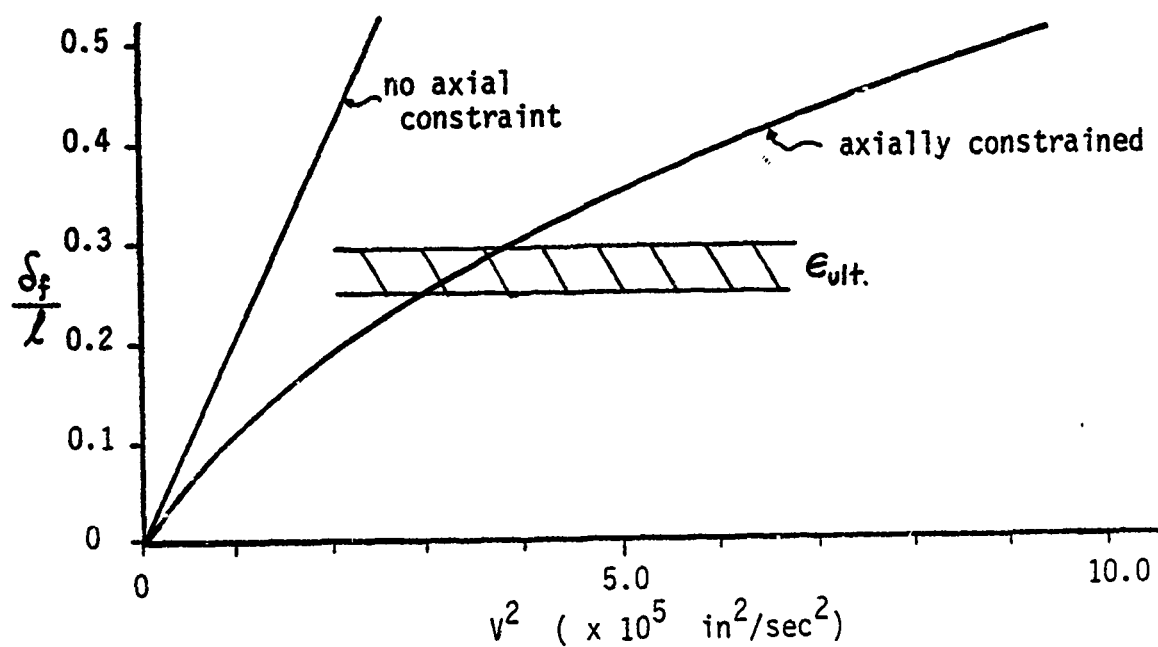(b) Constraints   (From reference 18)

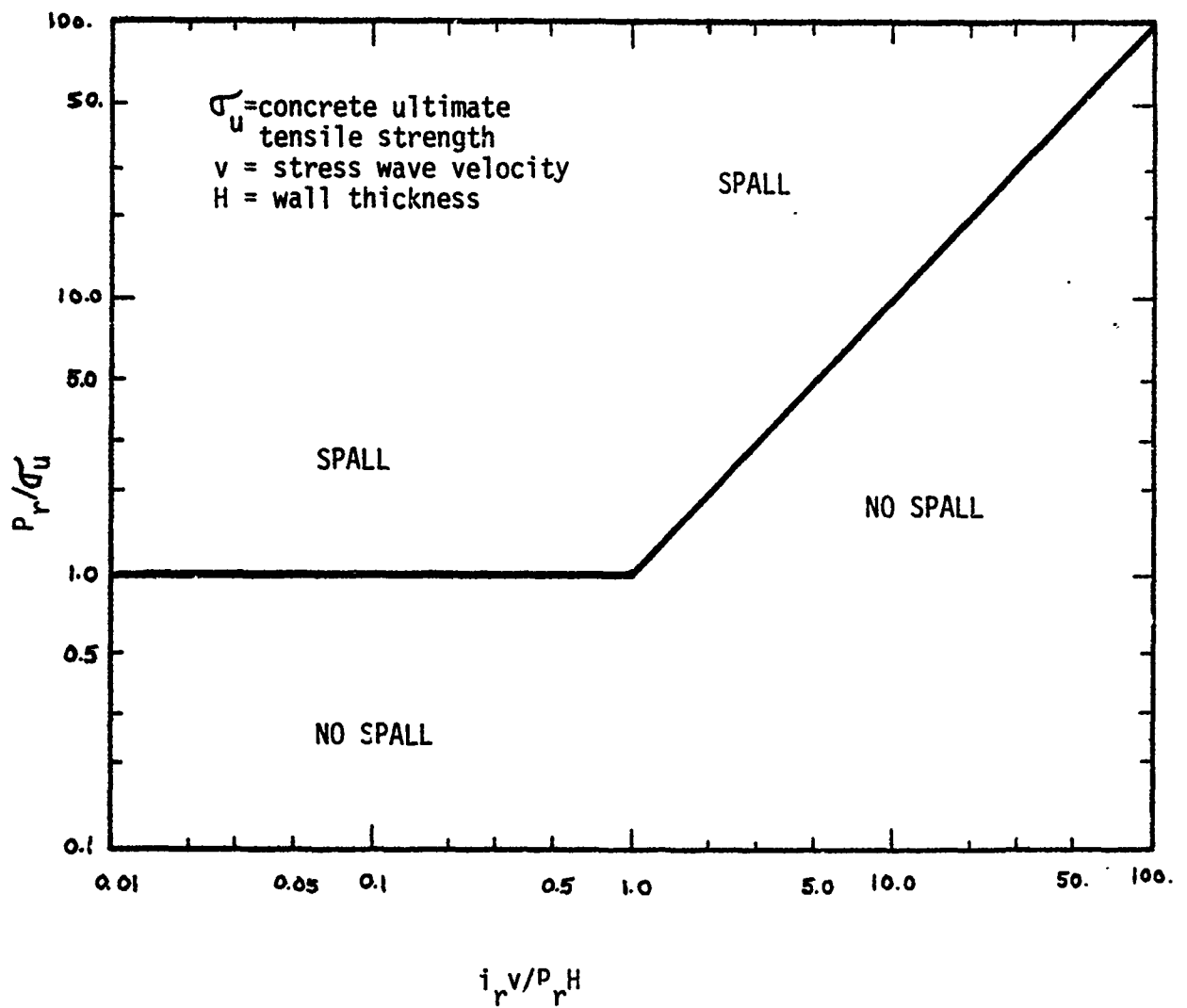Figure 6. Final Midspan Deflections for Example Problem

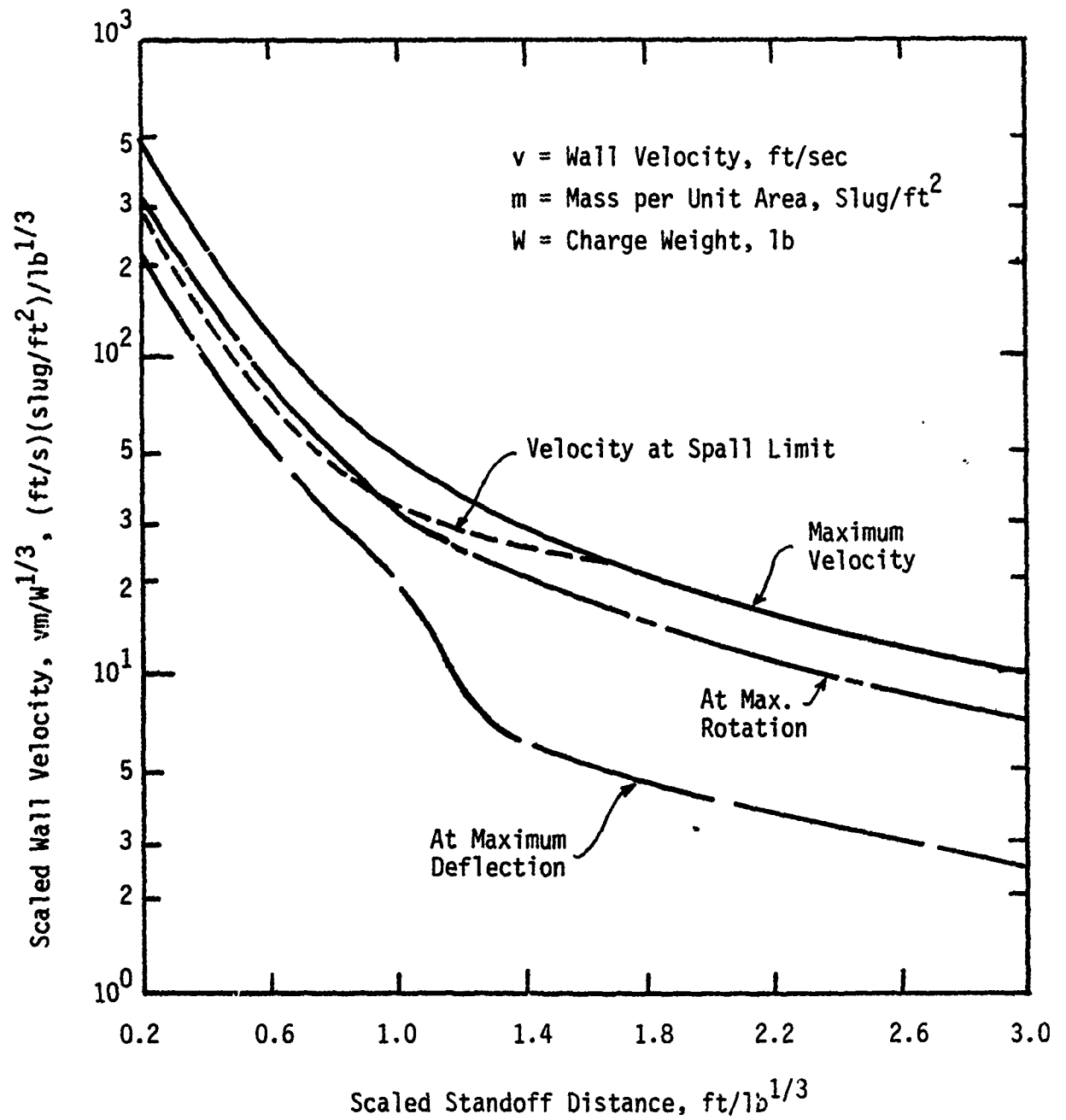Figure 7. Spall Threshold for Blast Waves Loading Walls
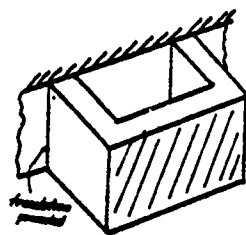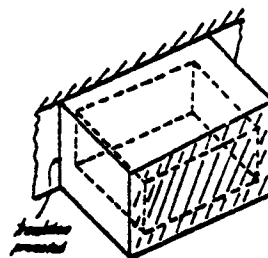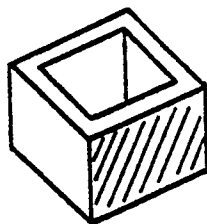(From reference 14)

Figure 8. Scaled Concrete Wall Velocities Due to Impulsive
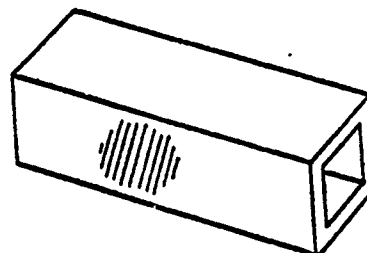Air Blast Loading (From Reference 16)

Type 1: Two Legged Support   Type 2: Four Legged Support

Type 3: Open Ended Box   Type 4: Box Structure
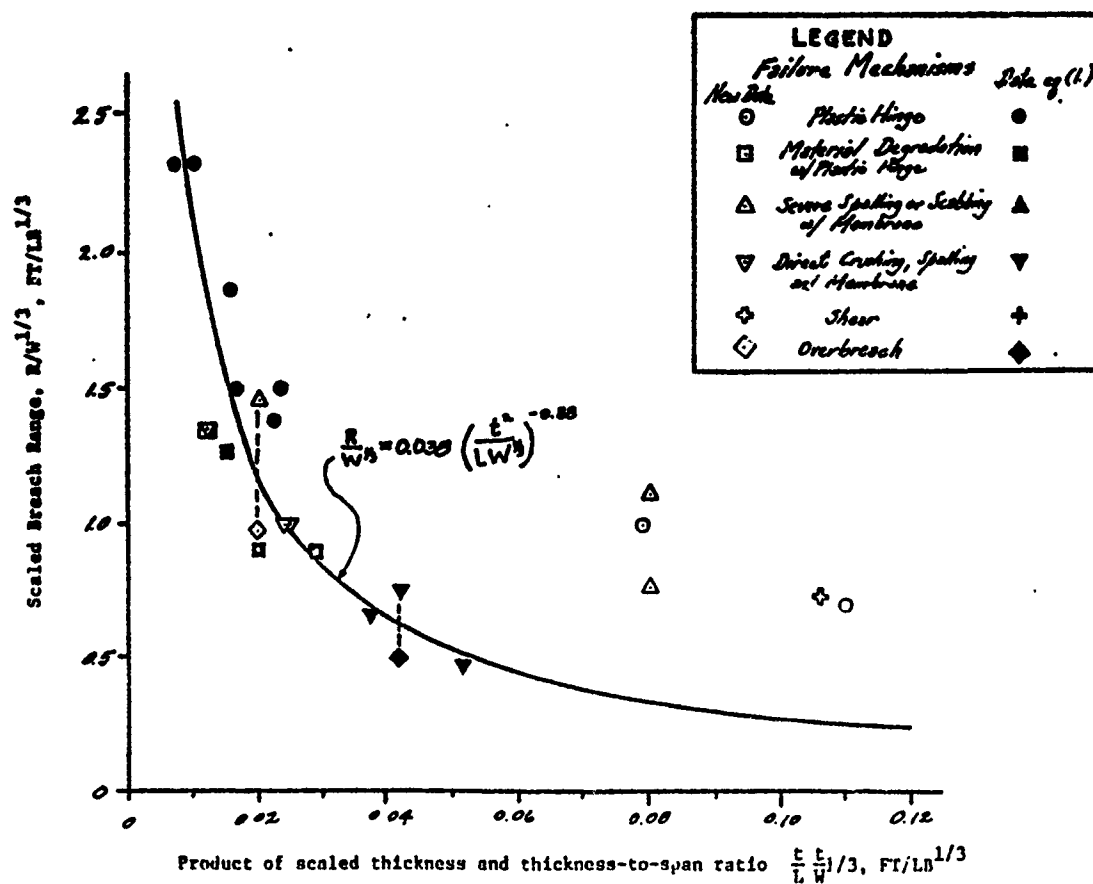
Figure A1. Support for Slab Specimens

Figure A2. Failure Mechanisms for Blast Loadings

43

Report Test No.	(lb/in³)	t (in)	ρ	L (ft)	f_c (ksi)	f_y (ksi)	R (ft)	W (lb)	λ (ft/lb)	Failure Mode	$\frac{t}{L}\frac{t}{W^{1/3}}$ (ft/lb^{1/3})	L/t	Explosive Type	Explosive Shape
AFATL-TR-77-115														
3	1	4.0	0.0050	3.33	>6.0	>49.5	2.0 / 1.5	4.64	4.20 / 0.90	2	0.0200	10.0	C-4	8
5	1	4.0	0.0050	3.33	>6.0	>47.5	3.0	7.94	1.50	1	0.0167	10.0	C-4	8
7	1	4.0	0.0050	3.33	>6.0	>47.5	4.0	10.00	1.86	1	0.0155	10.0	C-4	8
9	1	4.0	0.0050	2.33	>6.0	>47.5	2.0 / 1.5	4.64	4.20 / 0.90	2	0.0286	7.0	C-4	8
11	1	4.0	0.0050	2.33	>6.0	>47.5	3.0	7.94	1.50	1	0.0238	7.0	C-4	8
13	1	4.0	0.0050	2.33	>6.0	>47.5	3.0	10.00	1.39	1	0.0222	7.0	C-4	8
17	1	4.0	0.0050	1.33	>6.0	>47.5	1.0	7.94	0.50	6	0.0418	4.0	C-4	8
19	1	4.0	0.0050	5.33	>6.0	>47.5	5.0	12.00	2.32	1	0.0097	16.0	C-4	8
20	1	4.0	0.0050	5.33	>6.0	>47.5	7.0	27.00	2.33	1	0.0069	16.0	C-4	8
AFATL-TR-77-1 Vol. II														
10	2	8.0	0.0063	4.90	>6.0	Grade 40	1.0	10.00	0.46	4	0.0516	6.0	C-4	8
15	2	8.0	0.0063	4.90	>6.0	Grade 40	2.0	27.00	0.67	4	0.0370	6.0	C-4	8
21	2	4.0	0.0050	4.00	>6.0	Grade 40	2.0	4.00	1.26	2	0.0175	12.0	C-4	8

Table 1. Experimental Failure Data for Breach Equation of Reference 3.

Report Test No.	(lb/in³)	t (in.)	ρ	L (ft)	f_c (ksi)	f_y (ksi)	R (ft)	W (lb)	λ (ft/lb)	Failure Mode	$\frac{t}{L}\frac{t}{W^{1/3}}$ (ft/lb^{1/3})	L/t	Explosive Type	Explosive Shape
WES-TR-51-60-1														
3-3C	4	5.6	0.0089	4.0	6.5	>70	4.0	21.0	1.45	3	0.0200	8.6	TNT	sph.
5-3C	4	5.6	0.0089	4.0	6.5	>70	2.7	21.0	0.98	6	0.0200	8.6	TNT	sph.
8-3D	4	13.0	0.0085	4.0	6.5	>70	2.0	21.0	0.73	5	0.1060	3.7	TNT	sph.
AFATL-TR-78-92														
17	1	8.0	0.0025	2.8	>6.0	75	1.0	3.0	0.67	1	0.110	4.2	C-4	8
19	1	8.0	0.0025	2.8	>6.0	75	2.0	8.0	1.00	1	0.079	4.2	C-4	8
3	3	4.0	0.0050	2.33	>6.0	75	2.0	8.0	1.00	4	0.024	7.0	C-4	8
6	3	4.0	0.0050	2.33	>6.0	75	4.0	27.0	1.33	4	0.016	7.0	C-4	8
8	3	4.0	0.0050	2.33	>6.0	75	4.0	27.0	1.33	2	0.016	7.0	C-4	8
10	3	4.0	0.0050	2.33	>6.0	75	2.0	8.0	1.00	4	0.024	7.0	C-4	8
AFATL-N-77-8														
1	4	12.0	0.0092	4.00	4.0	Grade 40	3.50	31.0	1.11	3	0.080	4.0	AFX 108	cyl. cased
3	4	12.0	0.0092	4.00	4.0	Grade 40	2.42	31.0	0.77	3	0.080	4.0	AFX 108	cyl. cased
AFATL-TR-77-115														
16	1	4.0	0.0050	1.33	>6.0	>47.5	1.5	7.94	0.75	4	0.042	4.0	C-4	8

Table 2. Additional Failure Test Data